9

WSR-88D OBSERVATIONS OF AN EXTREME HAIL EVENT IMPACTING WESTERN SOUTH DAKOTA ON 20 JUNE 2015

ARTHUR WITT* AND JEFFREY C. SNYDER

NOAA/National Severe Storms Laboratory, Norman, OK

1. INTRODUCTION

On 20 June 2015, an intense supercell thunderstorm with hail to at least 15 cm in diameter (Fig. 1) impacted western South Dakota in the vicinity of Nisland. The storm produced widespread damage to vehicles, homes and businesses, with news reports of hailstones penetrating the shingle roofs of homes and the metal roofs of barns (Fig. 2). The storm occurred within 100 km of the KUDX WSR-88D (located near Rapid City). This study examined the character and evolution of the Nisland supercell hailstorm as seen by KUDX, in terms of overall storm intensity and a variety of dual polarization (DP) parameters.

2. DATA AND METHODS

a. Hailstone observations

There were six reports of large hail in or near Nisland (Fig. 3) between 0200 UTC and 0230 UTC in the Storm Prediction Center's log of storm reports (Storm Prediction Center 2015), with five of the six reports >6 cm in diameter and three reports >11 cm in diameter (Table 1). As is often the case with hail reports received from the general public, there were errors with the times for four of the reports based on refectivity data from KUDX (this is a well-known problem; Witt et al. 1998b; Blair et al. 2011). When necessary, the report times were adjusted using the 0.5° KUDX scans of reflectivity Z, differential reflectivity Z_{DR} and copolar correlation coefficient ρ_{HV} to produce a radar-based best estimate for the time when the hail observation most likely occurred.

b. Radar-based parameters

Storm intensity was assessed via three radar parameters. The two velocity-based parameters were derived from the radial velocity data, with the reflectivity parameter determined after "mapping" the radial reflectivity data to a 3D latitude-longitude-height grid at a resolution of 0.01° x 0.01° x 1.0 km (Lakshmanan et al. 2006). The reflectivity-based parameter examined was the maximum expected size of hail (MESH; Witt et al. 1998a; Lakshmanan et al. 2007). The two velocity-based parameters examined were the maximum storm-top divergent outflow (STD; Witt and Nelson 1991) and maximum mid-altitude rotational velocity (MRV; Witt 1998), with mid-altitude being 3–11 km above radar level (ARL). The equations for STD and MRV are:

$$STD = V_{Dmax} - V_{Dmin} \tag{1}$$

$$MRV = (V_{Rmax} - V_{Rmin})/2 \tag{2}$$

where V_{Dmin} and V_{Dmax} are the peak inbound and outbound velocities in the storm-top divergent signature, and V_{Rmin} and V_{Rmax} are the peak inbound and outbound velocities in the mid-altitude rotation signature within the storm. To focus the calculation of MRV on rotation versus divergence, the line connecting the locations of V_{Rmin} and V_{Rmax} needed to be more perpendicular than parallel to the radar viewing direction [i.e., have an angle >45°; see section 4.7 in Brown and Wood (2007)]. To minimize errors in the calculation of STD and MRV, only manually-dealiased radial velocity data with corresponding reflectivity $\geq$ 15 dBZ and spectrum width < 13 m s^{-1} were used. To avoid use of unreliable data, an additional criterion was that a candidate velocity have sufficient spatial continuity with neighboring velocities on the same elevation scan, defined here as at least one adjacent velocity value within 5 m s^{-1} of the candidate velocity value. In the calculation of STD, to reduce the altitude difference between V_{Dmin} and V_{Dmax}, V_{Dmin} could come from either the same or higher elevation scans as V_{Dmax}. Parameter V_{Dmin} at higher elevation scans (than V_{Dmax}) was primarily used to minimize the height difference between it and V_{Dmax} (so that the STD calculation was as close as possible to measuring horizontal divergence).

Corresponding author address: Arthur Witt, NOAA/National Severe Storms Laboratory, 120 David L. Boren Blvd., Norman, OK, 73072.
E-mail: Arthur.Witt@noaa.gov

TABLE 1. List of the six severe hailstone reports and associated HSDA observations, with SH indicating small hail and GH indicating giant hail.

Report nbr	Radar-based time (UTC)	SPC reported time (UTC)	Latitude (°)	Longitude (°)	Size (mm)	HSDA result	Distance to nearest GH area (km)
1	0208	0213	44.77	-103.59	44	GH	0
2	0213	0230	44.67	-103.59	64	SH	1.9
3	0215	0210	44.67	-103.55	114	SH	1.4
4	0220	0220	44.65	-103.5	152	SH	3.3
5	0220	0220	44.67	-103.47	114	SH	4.5
6	0226	0230	44.6	-103.43	70	SH	9.7

The low-altitude DP data above the locations of the hail reports were examined as the storm passed over these locations. The DP data analyzed included Z, Z_{DR}, ρ_{HV}, and specific differential phase (K_{DP}) (see Kumjian 2013, for a description of the polarimetric radar variables). Measures of these variables on the lowest elevation scan (0.5°) were calculated using the median value of the eight radar bins within a 1° x 1 km window centered on the location of the hail report. Given an update rate of $\sim$3 min for the lowest elevation scan (KUDX was scanning in Volume Coverage Pattern 212 combined with one supplemental 0.5° intra-volume elevation scan), it was sometimes necessary to extrapolate the position of the 1° x 1 km window based on storm motion to the closest scan, in time, to when the storm core passed over the location of the hail report. Also examined was the hydrometer classification algorithm (HCA; Park et al. 2009) indication of hydrometer type from the 0.5° elevation scan for the six hail reports. This classification included the new hail size discrimination algorithm (HSDA; Ortega et al. 2016) categories of small hail (SH; <25 mm), large hail (LH; 25–50 mm) and giant hail (GH; >50 mm).

A series of mid-altitude polarimetric signatures were also examined. These included Z, Z_{DR}, ρ_{HV}, K_{DP} and depolarization ratio (DR), along with commonly observed volumetric signatures such as Z_{DR} and K_{DP} columns as in or similar to Snyder et al. (2015). In addition, several experimental fields were produced and examined. The fields included Z_{DR} and ρ_{HV} at -10°C, -20°C, -30°C, and -40°C. From these, swaths of minimum and maximum Z_{DR} and ρ_{HV} at these discrete temperature levels and in the -20°C to -40°C layer were created.

3. RADAR OBSERVATIONS

a. Character and evolution of storm intensity

The first radar echo of the Nisland hailstorm (as seen from KUDX) occurred at 2030 UTC over SE Montana (located 306° and 373 km from KUDX). Given an environment supportive of rapid thunderstorm growth (Fig. 4), the storm quickly strengthened, with MESH increasing to 5 cm at 2051 UTC. The overall storm intensity, as measured by MESH, stayed around this magnitude as the storm propagated east-southeastward toward South Dakota, with MESH oscillating between 3–7 cm. As the storm approached the Montana/South-Dakota border around 0030 UTC (at a distance $\sim$160 km from KUDX), MESH was $\sim$5 cm, MRV was $\sim$30 m s^{-1} and STD was $\sim$90 m s^{-1} (Fig. 5). From 0031 UTC to 0045 UTC, there was a notable increase in STD from 90 m s^{-1} to 110 m s^{-1}. This preceded a sharp increase in MESH from 5 cm at 0044 UTC to 11 cm at 0056 UTC. Unfortunately, during the period of maximum MESH $\sim$11 cm from 0053–0104 UTC, it was not possible to accurately measure STD or MRV due to range-folding impacting the velocity data. However, shortly after the peak in MESH of 11.5 cm at 0104 UTC, an STD of 120 m s^{-1} was observed at 0106 UTC (Fig. 5). Following the peak in MESH and STD, there was a large decrease in MESH to a minimum of 3 cm at 0140 UTC, with a more modest decrease in STD to 93 m s^{-1} at 0132 UTC. Thereafter, another large increase in MESH and STD ocurred, with peaks of 10.7 cm at 0204 UTC for MESH and 138 m s^{-1} at 0214 UTC for STD. These peaks in MESH and STD ocurred shortly before the period of maximum reported hail size (Table 1). Although there were significant variations in MESH and STD from 0020–0230 UTC, MRV maintained a quasi-steady magnitude of 25–35 m s^{-1} throughout the time period. However, the maximum MRV of 35.6 m s^{-1} at 0219 UTC did occur at the same time as the maximum reported hail size of 15 cm.

b. Low-altitude dual-polarization observations

The relationship between the low-altitude DP observations (from the 0.5° elevation scans) and the hail reports were examined for Z, Z_{DR}, ρ_{HV}, and K_{DP}. The results show that the hail reports were associated with moderate to high Z ($\geq$54 dBZ), low Z_{DR} (<2 dB), and low-to-moderate ρ_{HV} (0.87–0.94) and K_{DP} (0.4–2.3° km^{-1}) (Fig. 6), with no apparent differences for hail sizes of 4–7 cm versus 11–15 cm. At the time and location of the six severe hail reports, the HCA/HSDA performed poorly, indicating SH for the five giant hail reports and GH for the

FIG. 1. Photographs of huge hailstones from the Nisland supercell.

FIG. 2. Photograph of a hole in the roof of a house impacted by the Nisland supercell.

FIG. 3. Geographic locations (black numerals) of the six severe hail reports in the vicinity of Nisland. See Table 1 for more details.

one large hail report (Table 1). However, for the five giant hail reports, GH was identified within 10 km of each report location.

c. Mid-altitude dual-polarization observations

Large hail tends to grow near strong updrafts, and the growth of large hail and/or the presence of hail of a par-

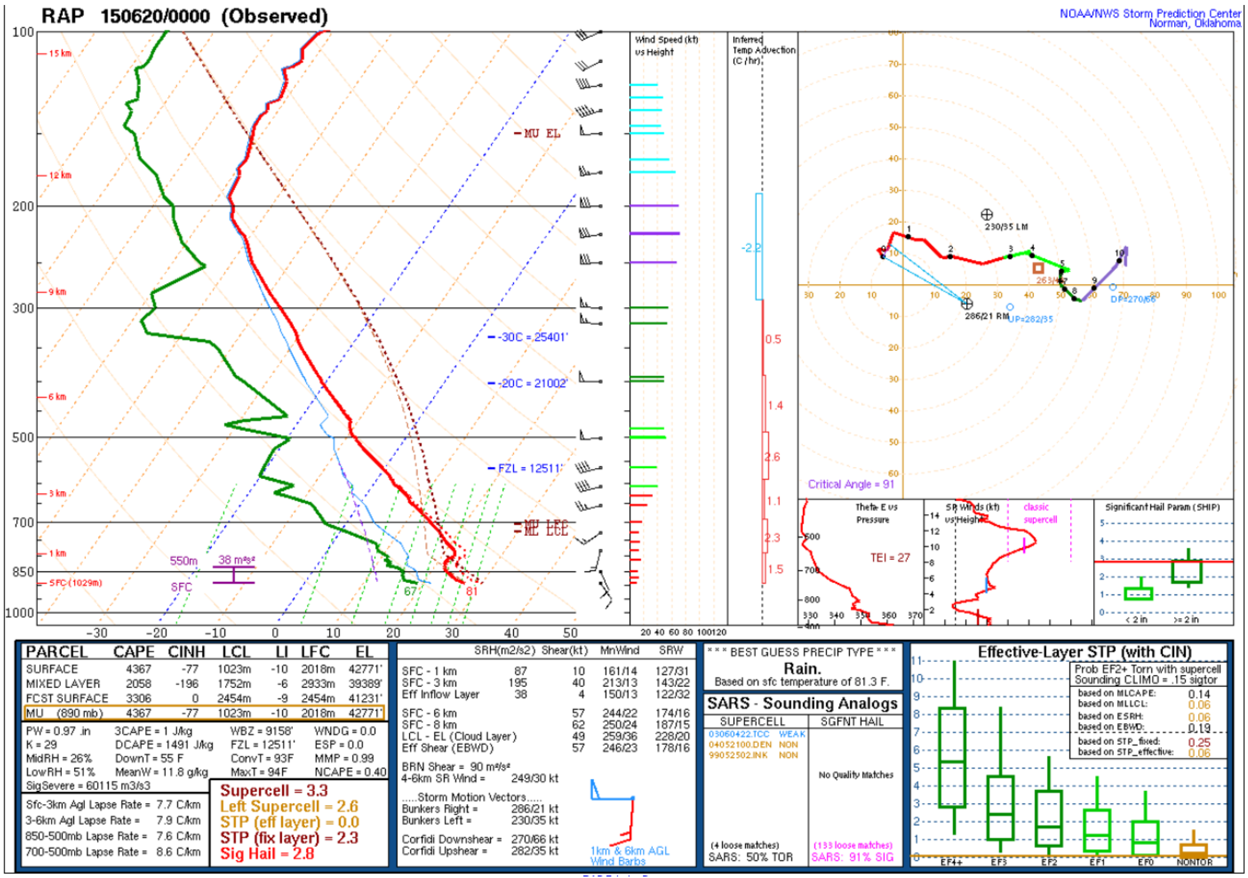

FIG. 4. RAP sounding at 0000 UTC 20 June 2015.

ticular size may give rise to two polarimetric signatures in the mid-altitudes of intense hailstorms: an area of reduced ρ_{HV} and a zone of negative Z_{DR} of -1 dB to -2 dB aloft. The Nisland supercell had both of these signatures before and during the times of the large hail reports. Fig. 7 shows the evolution of Z, Z_{DR} and ρ_{HV} from the 5.1° elevation scans during a 26 min period between 0200 UTC and 0226 UTC. A well-defined bounded weak echo region (BWER) is apparent in Z. An area of $Z_{DR} < -0.5$ dB is observed near and to the north and west of the BWER, though the height at which these observations were made decreased with time as the storm approached the radar. Also near to the north and west of the BWER was an area of reduced ρ_{HV}, at times dropping below 0.75 (e.g., at 0215 UTC). This appears to be very similar to the LoRB (low ρ_{HV} on the left and rear edge of the BWER) discussed in Snyder et al. (2013), itself similar to other observations in hail-producing storms (e.g., Hubbert et al. 1998; Kennedy et al. 2001).

Reconstructed vertical cross-sections from 0215 UTC (Fig. 8) highlight a number polarimetric signatures commonly observed in supercells (e.g., Kumjian and Ryzhkov 2008). A Z_{DR} column with maximum $Z_{DR} > 5$ dB extends to a height of ~6 km above radar level (ARL), above which Z_{DR} intermittently ranges from around -2 dB to 3 dB through ~9 km ARL. Essentially collocated with the Z_{DR} column and negative Z_{DR} region above the Z_{DR} column is an area of ρ_{HV} <0.95, with the minimum ρ_{HV} in this particular cross-section <0.75 between approximately 5 km and 7 km ARL. The net result of the Z_{DR} and ρ_{HV} signatures is a deep column of enhanced depolarization ratio (*DR*; Ryzhkov et al. 2017), prominently featured from nearly 3.5 km to 9 km ARL. There are at least two reasonable hypotheses to explain the reduced ρ_{HV} and negative Z_{DR} near and above the Z_{DR} column. First, it is possible that complex mixed-phase processes are producing hydrometeors with exotic shapes or uncommon orientations. Unfortunately, in-situ observations of hail growth in the updrafts of intense supercells are lacking. A second possibility is that there is a large amount of hail approximately 6 cm in diameter, a size at which resonance effects at S band may produce strongly negative Z_{DR}. Regardless, anecdotal observations by co-author J. Snyder indicate that convective storms that produce such large hail commonly have these polarimetric signatures aloft.

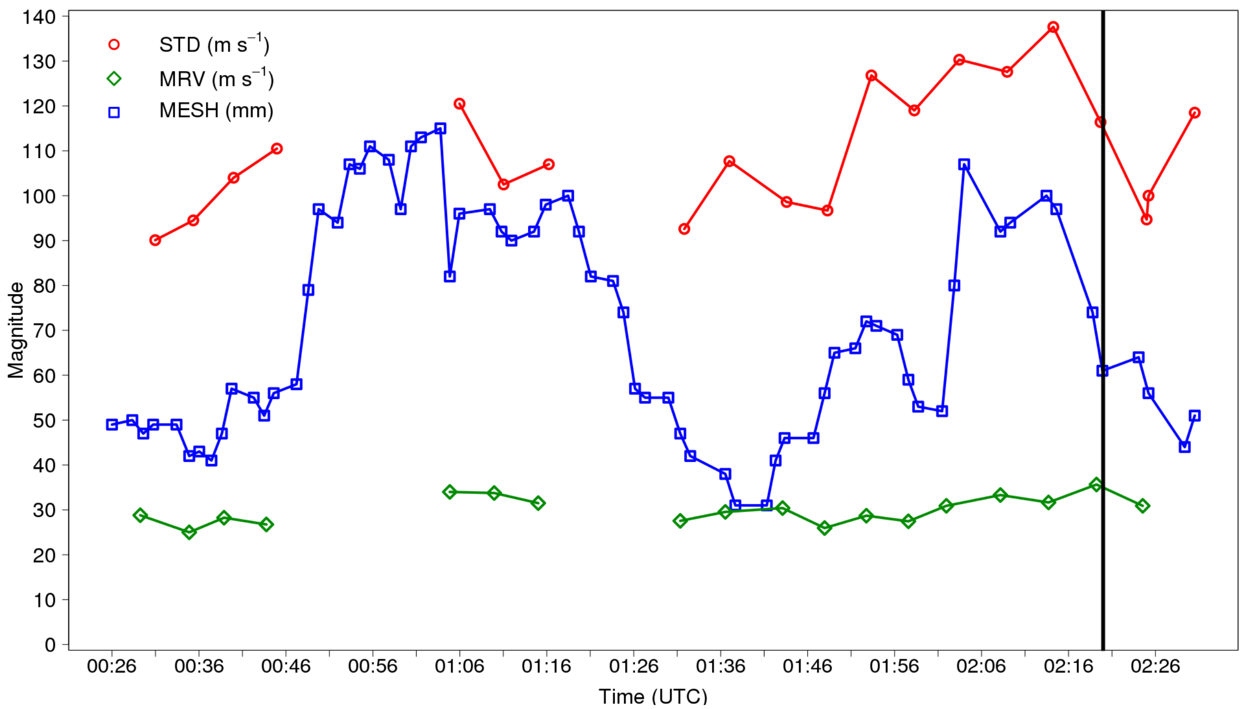

FIG. 5. Time series of STD, MRV, and MESH for the Nisland hailstorm from 0026–0231 UTC. The gaps in the STD and MRV time series are due to range-folding of the velocity data. The vertical black line indicates the time of the 15 cm hail report (0220 UTC).

Swaths or paths of polarimetric features of interest (Fig. 9) between 0145 UTC and 0230 UTC show potentially interesting patterns compared to the hail reports. For example, a swath of reduced ρ_{HV} at $-20°$C is noted very near the Z_{DR} column swath. Minimum ρ_{HV} at $-20°$C occurred to the east and southeast of Nisland, very near the location of the giant hail reports. Minimum Z_{DR} at $-40°$C during this time period also shows some similarities with the Z_{DR} column and ρ_{HV} swaths, though Z_{DR} less than -0.5 dB showed up before and to the northwest of the area of reduced ρ_{HV} (the different altitudes between these two products may explain some of this difference).

4. CONCLUSIONS

The damage potential and threat to life and property associated with a severe storm increases at a nonlinear rate as the intensity of the storm increases. Hence, timely identification and warning on the occurrence of extreme severe-weather events, such as the extremely-large, damaging hail produced by the Nisland supercell, is vital. In that regard, during the time period 0–20 min prior to the 15 cm hailstone report, all three storm-intensity parameters examined (MESH, MRV and STD) attained magnitudes typically associated with a supercell capable of producing giant hail (>10 cm in diameter). However, only the STD suggested the potential for an extreme hail event, reaching a maximum value of 138 m s^{-1}, which is nearly double the median maximum value of 72 m s^{-1} from a dataset of STD observations of storms producing giant hail (Blair et al. 2011). It is also possible that the actual STD was undersampled due to the coarser vertical resolution of VCP-212 compared with higher resolution scanning strategies often used by research radars (e.g., Witt and Kuster 2017; Witt et al. 2018). Although not as extreme as the STD, the mesocyclone midaltitude rotational velocity (MRV) maximum value of 35.6 m s^{-1} was also notably higher than the median value of 24.5 m s^{-1} within storms producing giant hail (Blair et al. 2011).

The low-altitude DP observations associated with the six severe hail reports were generally consistent with previous studies of large hail at 10-cm wavelength, namely high Z, low Z_{DR}, and low-to-moderate ρ_{HV} and K_{DP} (Payne et al. 2010; Picca and Ryzhkov 2012; Smyth et al. 1999; Snyder et al. 2014). At the time and location of the six hail reports, the HCA/HSDA performed poorly, indicating SH for the five giant hail reports and GH for the one large hail report. The poor performance for the giant hail reports is likely due to Z_{DR} being higher at those locations than the HSDA typically classifies for GH. However, for all the giant hail reports, GH was identified in nearby areas of the storm.

The Nisland supercell possessed several of the commonly observed mid-altitude polarimetric signatures associated with hail-producing supercells. The supercell was

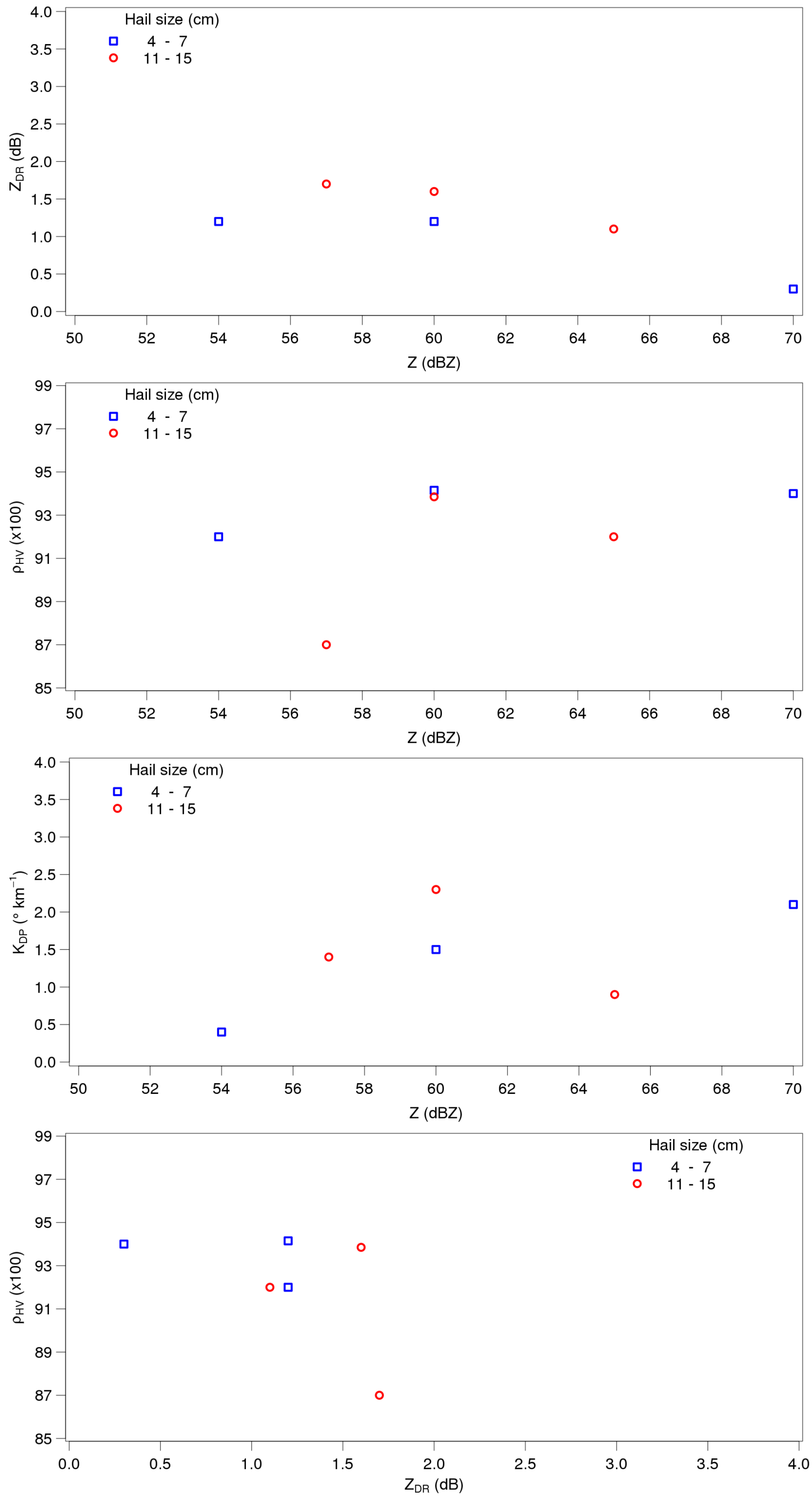

FIG. 6. KUDX observations from the 0.5° elevation scans of Z, Z_{DR}, ρ_{HV} and K_{DP} associated with the six hail reports.

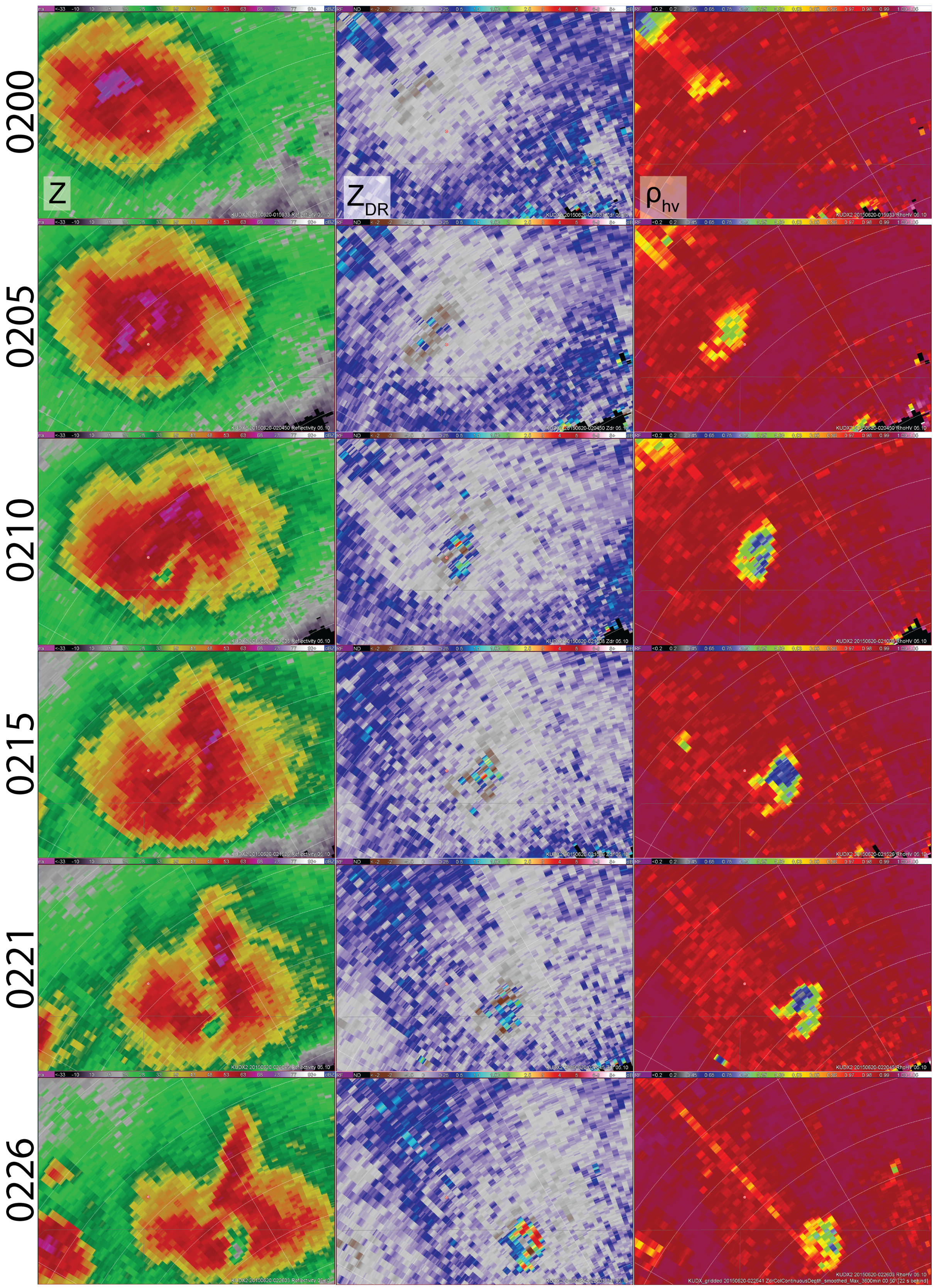

FIG. 7. KUDX observations from the 5.1° elevation scans of (left) Z, (center) Z_{DR} and (right) ρ_{HV} at ∼5 min intervals between 0200–0226 UTC. The time (in UTC) of each set of scans is shown on the far left.

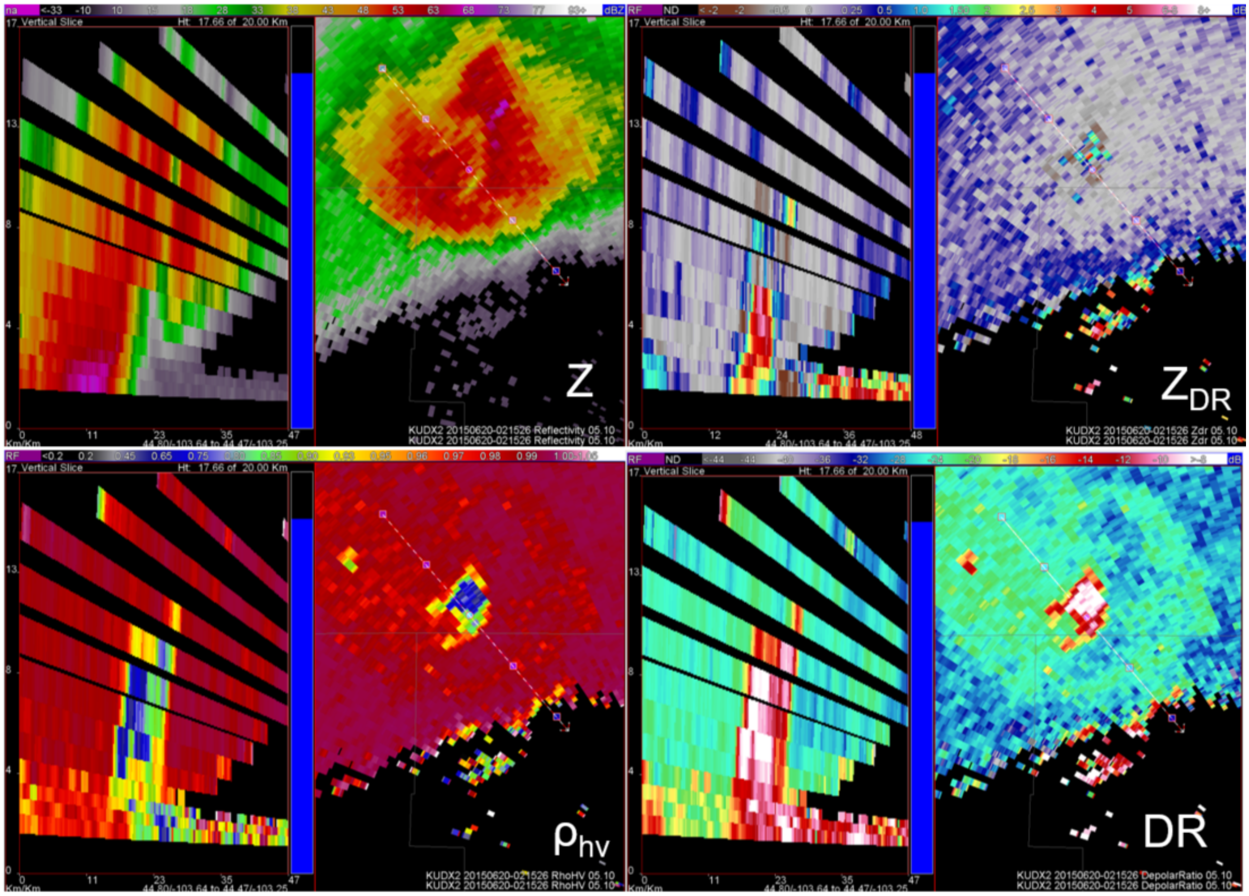

FIG. 8. Reconstructed vertical cross-sections (left part of each panel) and 5.1° elevation scans (right half of each panel) showing (clockwise from upper left) Z, Z_{DR}, DR and ρ_{HV} at 0215 UTC on 20 June 2015.

associated with a deep Z_{DR} column that was topped by a 2–3 km deep area of $Z_{\mathrm{DR}} < -1$ dB nearly collocated with reduced ρ_{HV} to ≤ 0.75. A preliminary analysis of several derived polarimetric fields interpolated to a series of temperature levels shows that the severe hail reports occurred near areas of reduced ρ_{HV} aloft and very near the path of the updraft as one can infer from the Z_{DR} column. Much work remains in further assessing the effectiveness of these products in nowcasting large and giant hail.

References

Blair, S. F., D. R. Deroche, J. M. Boustead, J. W. Leighton, B. L. Barjenbruch, and W. P. Gargan, 2011: A radar-based assessment of the detectability of giant hail. *E-Journal of Severe Storms Meteorology*, **6 (7)**, 1–30, [Available online at http://www.ejssm.org/ojs/index.php/ejssm/article/view/87.].

Brown, R. A., and V. T. Wood, 2007: A guide for interpreting Doppler velocity patterns: Northern Hemisphere edition. Tech. rep., NOAA/National Severe Storms Laboratory, Norman, OK, 61 pp. [Available online at https://www.nssl.noaa.gov/publications/dopplerguide/Doppler%20Guide%202nd%20Ed.pdf.].

Hubbert, J., V. N. Bringi, L. D. Carey, and S. Bolen, 1998: CSU-CHILL polarimetric radar measurements from a severe hail storm in eastern Colorado. *Journal of Applied Meteorology*, **37**, 749–775, doi:10.1175/1520-0450(1998)037⟨0749:CCPRMF⟩2.0.CO;2.

Kennedy, P. C., S. A. Rutledge, W. A. Petersen, and V. N. Bringi, 2001: Polarimetric radar observations of hail formation. *Journal of Applied Meteorology*, **40**, 1347–1366, doi:10.1175/1520-0450(2001)040⟨1347:PROOHF⟩2.0.CO;2.

Kumjian, M. R., 2013: Principles and applications of dual-polarization weather radar. Part I: Description of the polarimetric radar variables. *J. Operational Meteor.*, **1 (19)**, 226–242, doi:10.15191/nwajom.2013.0119.

Kumjian, M. R., and A. V. Ryzhkov, 2008: Polarimetric signatures in supercell thunderstorms. *J. Appl. Meteor. Climatol.*, **47**, 1940–1961, doi:10.1175/2007JAMC1874.1.

Lakshmanan, V., T. Smith, K. Hondl, G. J. Stumpf, and A. Witt, 2006: A real-time, three-dimensional, rapidly updating, heterogeneous radar merger technique for reflectivity, velocity, and derived products. *Wea. Forecasting.*, **21**, 802–823, doi:10.1175/WAF942.1.

Lakshmanan, V., T. Smith, G. Stumpf, and K. Hondl, 2007: The Warning Decision Support System – Integrated Information. *Wea. Forecasting.*, **22**, 596–612, doi:10.1175/WAF1009.1.

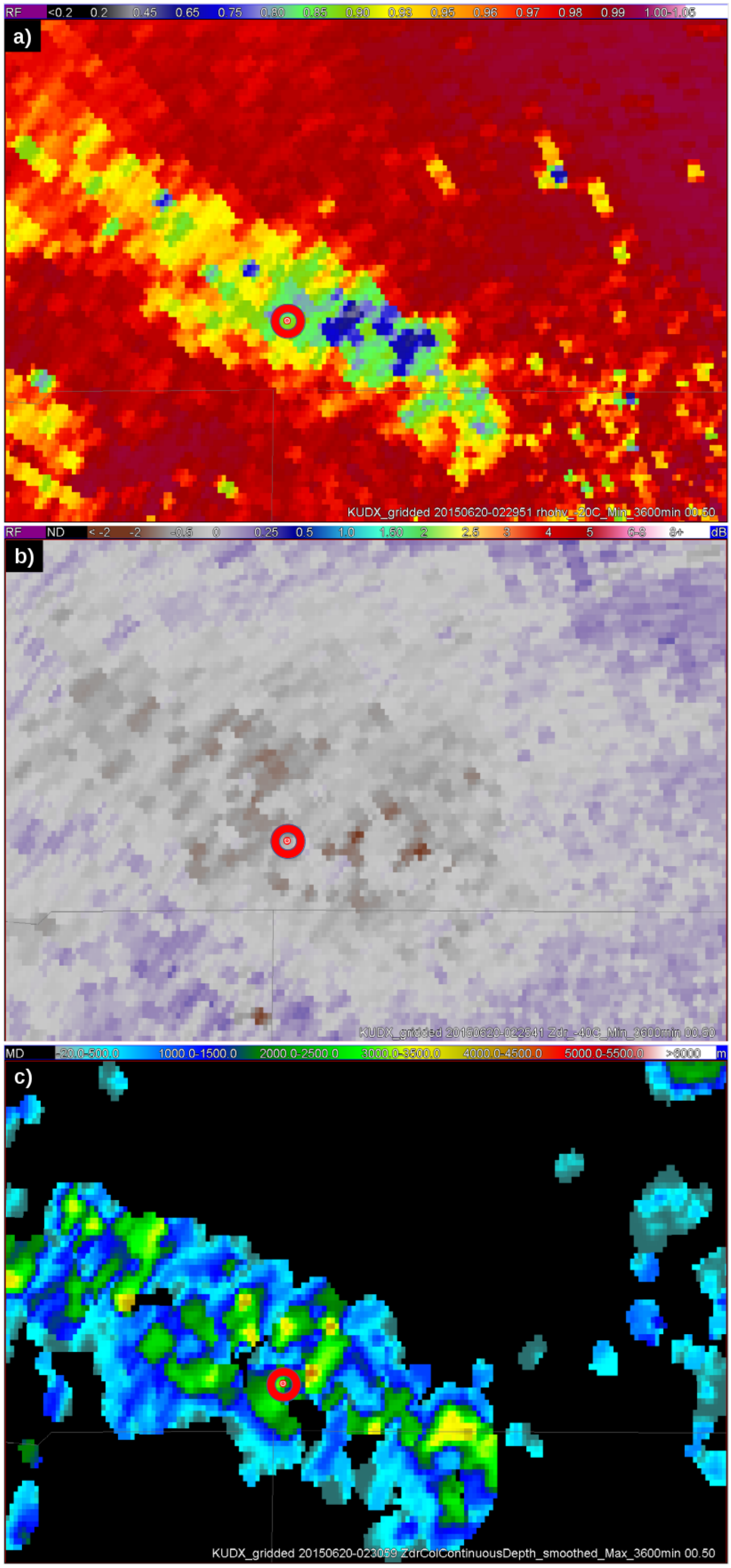

FIG. 9. Fields of (a) minimum ρ_{HV} at $-20°C$, (b) minimum Z_{DR} at $-40°C$, and (c) maximum Z_{DR} column height (above the environmental 0°C height) in the 0145–0230 UTC period. The red circle marks the location of Nisland, SD.

Ortega, K. L., J. M. Krause, and A. V. Ryzhkov, 2016: Polarimetric radar characteristics of melting hail. Part III: Validation of the algorithm for hail size discrimination. *Journal of Applied Meteorology and Climatology*, **55**, 829–848, doi:10.1175/JAMC-D-15-0203.1.

Park, H. S., A. V. Ryzhkov, D. S. Zrnić, and K.-E. Kim, 2009: The hydrometeor classification algorithm for the polarimetric WSR-88D: Description and application to an MCS. *Weather and Forecasting*, **24**, 730–748, doi:10.1175/2008WAF2222205.1.

Payne, C. D., C. A. V. D. Broeke, L. R. Lemon, and P. T. Schlatter, 2010: Polarimetric radar characteristics of a supercell hailstorm on 10 May 2010 in central Oklahoma. *Proc. 25th Conf. on Severe Local Storms*, Denver, CO, Amer. Meteor. Soc., P8.7, [Available online at https://ams.confex.com/ams/25SLS/techprogram/Paper_175763.htm.].

Picca, J., and A. Ryzhkov, 2012: A dual-wavelength polarimetric analysis of the 16 May 2010 Oklahoma City extreme hailstorm. *Mon. Wea. Rev.*, **140**, 1385–1403, doi:10.1175/MWR-D-11-00112.1.

Ryzhkov, A., and Coauthors, 2017: Estimation of depolarization ratio using weather radars with simultaneous transmission/reception. *Journal of Applied Meteorology and Climatology*, **56**, 1797–1816, doi:10.1175/JAMC-D-16-0098.1.

Smyth, T. J., T. M. Blackman, and A. J. Illingworth, 1999: Observations of oblate hail using dual polarization radar and implications for hail-detection schemes. *Quart. J. Roy. Meteor. Soc.*, **125**, 993–1016, doi:10.1002/qj.49712555512.

Snyder, J. C., H. B. Bluestein, V. Venkatesh, and S. J. Frasier, 2013: Observations of polarimetric signatures in supercells by an X-band mobile Doppler radar. *Monthly Weather Review*, **141**, 3–29, doi:10.1175/MWR-D-12-00068.1.

Snyder, J. C., A. V. Ryzhkov, H. B. Bluestein, and S. F. Blair, 2014: Polarimetric analysis of two giant-hail-producing supercells observed by X-band and S-band radars. *Proc. 27th Conf. on Severe Local Storms*, Madison, WI, Amer. Meteor. Soc., 166, [Available online at https://ams.confex.com/ams/27SLS/webprogram/Paper255455.html.].

Snyder, J. C., A. V. Ryzhkov, M. R. Kumjian, A. P. Khain, and J. Picca, 2015: A Z_{DR} column detection algorithm to examine convective storm updrafts. *Wea. Forecasting*, **30**, 1819–1844, doi:10.1175/WAF-D-15-0068.1.

Storm Prediction Center, 2015: Storm Reports. [Available online at https://www.spc.noaa.gov/climo/reports/150619_rpts.html.].

Witt, A., 1998: The relationship between WSR-88D measured midaltitude rotation and maximum hail size. Preprints, *19th Conference on Severe Local Storms*, Minneapolis, MN, Amer. Meteor. Soc., 740–743.

Witt, A., D. W. Burgess, A. Seimon, J. T. Allen, J. C. Snyder, and H. B. Bluestein, 2018: Rapid-scan radar observations of an Oklahoma tornadic hailstorm producing giant hail. *Weather and Forecasting*, **33**, 1263–1282, doi:10.1175/WAF-D-18-0003.1.

Witt, A., M. D. Eilts, G. J. Stumpf, J. T. Johnson, E. D. W. Mitchell, and K. W. Thomas, 1998a: An enhanced hail detection algorithm for the WSR-88D. *Wea. Forecasting.*, **13**, 286–303, doi:10.1175/1520-0434(1998)013⟨0286:AEHDAF⟩2.0.CO;2.

Witt, A., M. D. Eilts, G. J. Stumpf, E. D. W. Mitchell, J. T. Johnson, and K. W. Thomas, 1998b: Evaluating the performance of WSR-88D severe storm detection algorithms. *Wea. Forecasting.*, **13**, 513–518, doi:10.1175/1520-0434(1998)013⟨0513:ETPOWS⟩2.0.CO;2.

Witt, A., and C. M. Kuster, 2017: Rapid-scan dual-polarization WSR-88D observations of Oklahoma hailstorms on 26 march 2017. *Proc. 38th Conf. on Radar Meteorology*, Chicago, IL, Amer. Meteor. Soc., 224, [Available online at https://ams.confex.com/ams/38RADAR/meetingapp.cgi/Paper/320886.].

Witt, A., and S. P. Nelson, 1991: The use of single-Doppler radar for estimating maximum hailstone size. *J. Appl. Meteor.*, **30**, 425–431, doi:10.1175/1520-0450(1991)030⟨0425:TUOSDR⟩2.0.CO;2.